

# Shape Parameter Estimation

**Peng Zheng**

*Department of Applied Mathematics  
University of Washington  
Seattle, WA 98195-4322, USA*

ZHENGP@UW.EDU

**Aleksandr Y. Aravkin**

*Department of Applied Mathematics  
University of Washington  
Seattle, WA 98195-4322, USA*

SARAVKIN@UW.EDU

**Karthikeyan Natesan Ramamurthy**

*IBM T.J. Watson Research Center  
Yorktown Heights, NY USA*

KNATESA@US.IBM.COM

**Editor:**

## Abstract

Performance of machine learning approaches depends strongly on the choice of misfit penalty, and correct choice of penalty parameters, such as the threshold of the Huber function. These parameters are typically chosen using expert knowledge, cross-validation, or black-box optimization, which are time consuming for large-scale applications.

We present a principled, data-driven approach to simultaneously learn the model parameters and the misfit penalty parameters. We discuss theoretical properties of these joint inference problems, and develop algorithms for their solution. We show synthetic examples of automatic parameter tuning for piecewise linear-quadratic (PLQ) penalties, and use the approach to develop a self-tuning robust PCA formulation for background separation.

## 1. Introduction

When designing machine learning formulations, choice of penalty plays a key role in the accuracy of the inferred model, and robustness of the learning procedure. Consider Figure 1, where data from a simple linear regression has been contaminated with asymmetric outliers.

The data generating mechanism is shown in black. The linear regression model for the data  $\{y_i, a_i\}$  is given by

$$y = \langle a_i, x \rangle + \epsilon_i, \quad (1)$$

with  $\epsilon_i$  assumed i.i.d. Gaussian variables. The maximum likelihood formulation is

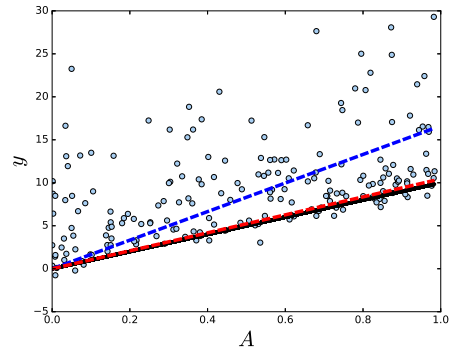


Figure 1: Linear regression with contaminated data: true model (black), linear regression estimate (blue dash) and penalty-tuned estimate (red dash).

equivalent to the least square problem,

$$\min_x \frac{1}{2} \|Ax - y\|^2.$$

This assumption is violated in Figure 1; the data are corrupted with asymmetric errors, and contain outliers. The least squares fit, shown in blue dash, fails to detect the true data generating mechanism.

To learn effectively in these cases, we consider a parameterized family of penalties  $\rho(x; \theta)$ , where  $x$  are model parameters and  $\theta$  control the shape of the penalty. The family is rich enough to allow the kinds of errors in Figure 1, and we learn  $x$  and  $\theta$  simultaneously using an extended statistical model.

Two immediate examples of  $\theta$  are the robustness threshold  $\kappa$  in the Huber penalty, and the slope  $\tau$  in the asymmetric quantile penalty, see Figure 2. Selecting the appropriate  $\theta$  is important. The quantile Huber case was considered by Ramamurthy et al. (2015). For example, the fit with the correctly set quantile penalty is shown in red dash in Figure 1. The value of  $\tau$  was obtained automatically from the data using a statistical model detailed in Section 2, and did not require cross-validation. The main focus of this paper is data-drive approaches for simultaneously selecting  $\theta$  and solving for  $x$ , without cross-validation or prior/additional information.

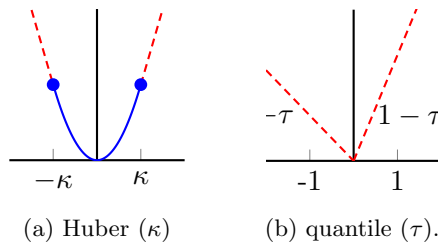


Figure 2: Huber and quantile penalties are parametrized by  $\kappa$  and  $\tau$ .

## 1.1 Related work

Meta-parameters are classically estimated using cross-validation or grid search. These methods typically require multiple solutions of any given learning problem, where a held-out dataset is used to evaluate each configuration. More recently, Bayesian optimization (Snoek et al., 2012; Hutter et al., 2011; Bergstra et al., 2011; Klein et al., 2016) and random search (Bergstra and Bengio, 2012; Li et al., 2016) have come to the forefront as two leading techniques that can be used to obtain meta-parameters in a very wide range of contexts.

All of these techniques can also be used for the problem class we consider. However, applying these approaches is always more computationally expensive than solving a single instance of a learning problem; both random search and Bayesian optimization require many instance evaluations. In contrast, for the narrower context of shape parameter estimation, we solve a *single* extended problem to simultaneously fit the  $x$  and  $\theta$ .

The most relevant works related to this paper focus on the relation between the quantile penalty and the asymmetric Laplace distribution (ALD) (Yu and Moyeed, 2001; Tu et al., 2017; Bera et al., 2016). Bera et al. (2016) jointly estimate the model and the shape parameters for quantile penalty, and Tu et al. (2017) infer the joint posterior distribution of these parameters.

## 1.2 Contributions

We develop a maximum-likelihood approach to simultaneously learn both the model and shape parameters for a broad class of penalties, of which the quantile is one example. The likelihood is obtained by interpreting each penalty as a statistical density, with normalization constant depending on the shape parameters  $\theta$ . The modeling innovation is to systematically incorporate the log of the normalization constant into the joint inference problem:

$$\min_{x, \theta \in \mathcal{D}} \rho(x; \theta) + g(x) + l(\theta). \quad (2)$$

Here,  $g(x)$  is any regularization term on  $x$ , while  $l(\theta)$  is the log of the normalization constant that arises from the statistical model, and ensures the model remains statistically valid as  $\rho$  is adapted.

Our second contribution is algorithmic. We consider first-order schemes, and show how to apply the PALM (Bolte et al., 2014) algorithm to problem (2). The PALM algorithm is limited to penalties  $\rho$  that are smooth in  $(x, \theta)$ , and so we design a new second-order interior point algorithm for problems with non-smooth coupling. The approach and algorithms are illustrated using synthetic and real data.

## 1.3 Roadmap

The paper proceeds as follows. In Section 2 we derive the maximum likelihood model for joint inference in  $x$  and  $\theta$  and characterize theoretical properties of the resulting objectives from an optimization perspective. In Section 3, we consider first- and second-order algorithms for the structured but generally nonconvex and nonsmooth objective (2). Section 4 illustrates the convergence rates of the methods, as well as behavior of the shape-tuned estimates, using synthetic data. In Section 5, we develop self-tuning RPCA approaches, and apply them to real data.

## 2. Statistical Model and Properties of Joint Objective

Penalties in learning formulations have underlying statistical assumptions. In this section we first review the relationship between penalties and corresponding residual distributions. We then use this relationship to develop a joint maximum likelihood approach for model and shape parameter inference, and characterize properties of the resulting objective function.

### 2.1 Statistical view

Recall the quantile penalty in Figure 2. If we choose  $\tau$  to be close to 1, we penalize the negative errors a lot more than the positive. Equivalently, we assume that the distribution of the errors  $\epsilon_i$  is biased towards positive errors.

The relationship between penalties and associated densities can be made precise. Given a penalty  $\rho(r; \theta)$ , we assume  $\epsilon_i$  in (1) are i.i.d. samples from the distribution with density

$$p(r; \theta) = \frac{1}{n_c(\theta)} \exp[-\rho(r; \theta)], \quad \text{where} \quad n_c(\theta) = \int_{\mathbb{R}} \exp[-\rho(r; \theta)] dr. \quad (3)$$

The term  $n_c(\theta)$  is a normalization constant that ensures that  $\rho(r, \theta)$  can be interpreted as a density as in (3). We can now formulate the *joint* maximum likelihood problem in  $(x, \theta)$ , or equivalently minimize its negative log:

$$\min_{x, \theta \in \mathcal{D}} \sum_{i=1}^m \rho(y_i - \langle a_i, x \rangle; \theta) + g(x) + m \log[n_c(\theta)]. \quad (4)$$

The parameter  $\theta$  may be restricted to a domain  $\mathcal{D}$ ; for example, the slope parameter  $\tau$  must be between 0 and 1 (see Figure 2). The term  $g(x)$  is an optional regularization function, e.g.  $\lambda \|x\|_1$  or indicator of  $x \in \mathcal{C}$  for some set  $\mathcal{C}$ .

The objective in the quantile example used to obtain the penalty-tuned fit in Figure 1 is given by

$$\min_{x, \tau \in [0, 1]} q_\tau(Ax - b) + m \log \left( \frac{1}{\tau} + \frac{1}{1 - \tau} \right), \quad (5)$$

with  $q_\tau$  the asymmetric 1-norm, and  $m$  the length of the residual. In this special case,  $\log(n_c)$  is available in closed form, is smooth in the interior of its domain, and acts as a barrier function for the interval  $[0, 1]$  that favors  $\tau = 0.5$ . It's also a strongly convex function, but has *no global quadratic upper bound*, violating a key assumption often required by optimization algorithms. In the remainder of this section, we characterize theoretical properties of the objective (4).

## 2.2 Theoretical properties

Smoothness, convexity, and quadratic upper bounds are at the center of algorithm design, and understanding these properties guide the choice of algorithms for (4).

**Assumption 1** *To ensure the validity of the statistical viewpoint, we require  $\rho$  to satisfy:*

1.  $\rho(r; \theta) \geq 0$ , for every  $\theta \in \mathcal{D}$  and  $r \in \mathbb{R}$  (**non-negativity**)
2. For any  $\theta \in \mathcal{D}$ ,  $n_c(\theta) = \int_{\mathbb{R}} \exp[-\rho(r; \theta)] dr < \infty$  (**integrability**)
3. For any  $\theta_0 \in \mathcal{D}$ ,  $\rho(r; \theta)$  is  $C^2$  around  $\theta_0$  for almost every  $r \in \mathbb{R}$  (**smoothness in  $\theta$** )

Under these assumptions, we can obtain formulas for the first and second derivatives of  $n_c(\theta)$ .

**Theorem 1 (smoothness of  $n_c(\theta)$ )** *For  $n_c(\theta)$  in (3), suppose Assumption 1 holds and for  $\theta_0 \in \mathcal{D}$ , there exist functions  $g_k(r)$ ,  $k = 1, 2$ , such that,*

1. for any unit vector  $v$ ,  $|\langle \nabla_\theta \exp[-\rho(r; \theta)], v \rangle| \leq g_1(r)$  for any  $\theta$  around  $\theta_0$ ,
2. for any unit vector  $v$ ,  $|\langle \nabla_\theta^2 \exp[-\rho(r; \theta)] v, v \rangle| \leq g_2(r)$  for any  $\theta$  around  $\theta_0$ ,
3.  $\int_{\mathbb{R}} g_k(r) dr < \infty$ ,  $k = 1, 2$ .

then  $n_c(\theta)$  is  $C^2$  continuous around  $\theta_0$  and,

$$\nabla n_c(\theta_0) = \int_{\mathbb{R}} \nabla_\theta \exp[-\rho(r; \theta_0)] dr, \quad \nabla^2 n_c(\theta_0) = \int_{\mathbb{R}} \nabla_\theta^2 \exp[-\rho(r; \theta_0)] dr. \quad (6)$$

The proof is straightforward, and included in the supplementary materials. The derivative formulas (6) are used for first- and second-order methods to infer  $x$  and  $\theta$ . The parametrization conditions in  $\theta$  are satisfied by all commonly used piecewise linear quadratic (PLQ) examples (Aravkin et al., 2013), including Huber and quantile penalties in Figure 2.

The theorem applies more generally to densities that are not log-concave. For example, the Student's  $t$  density and associated penalty satisfy Assumption 1 and other assumptions of Theorem 1 for  $\nu > 1$ .

In the quantile case (5), the term  $\log[n_c(\theta)]$  is convex. We characterize sufficient conditions for convexity of  $\log[n_c(\theta)]$  for a general class of penalties  $\rho$ .

**Theorem 2 (convexity of  $\log[n_c(\theta)]$ )** *Consider same definition of  $n_c(\theta)$  in Theorem 1, and suppose Assumption 1 holds. We have the following results:*

1. *If  $\rho(r; \theta)$  is jointly convex in  $r$  and  $\theta$ , then  $\log[n_c(\theta)]$  is a concave function of  $\theta$ .*
2. *If  $\rho(r; \theta)$  is concave with respect to  $\theta$  for every  $r$ , then  $\log[n_c(\theta)]$  is a convex function.*

This result follows from (Boyd and Vandenberghe, 2004, Chapter 3.5).

Theorems 1 and 2 tell an interesting story. The log-normalization constant  $\log[n_c(\theta)]$  is nearly always smooth; even when the loss  $\rho$  is nonsmooth in  $x$ . The inference problem (4) is *never jointly convex* in  $(x, \theta)$ ; in particular looking for a jointly convex formulation  $\rho(x; \theta)$  guarantees  $\log[n_c(\theta)]$  will be *concave*. This is intuitive, as we are attempting to learn both the model and error structure at the same time. Objective (4) is, in general, nonsmooth and nonconvex; but it has a fairly simple structure that is exploited to design first and second order methods in the next section.

To understand how non-convex (4) is, we apply partial minimization, and consider the function

$$\varrho(\theta) = \min_x \sum_{i=1}^m \rho(y_i - \langle a_i, x \rangle; \theta) + m \log[n_c(\theta)].$$

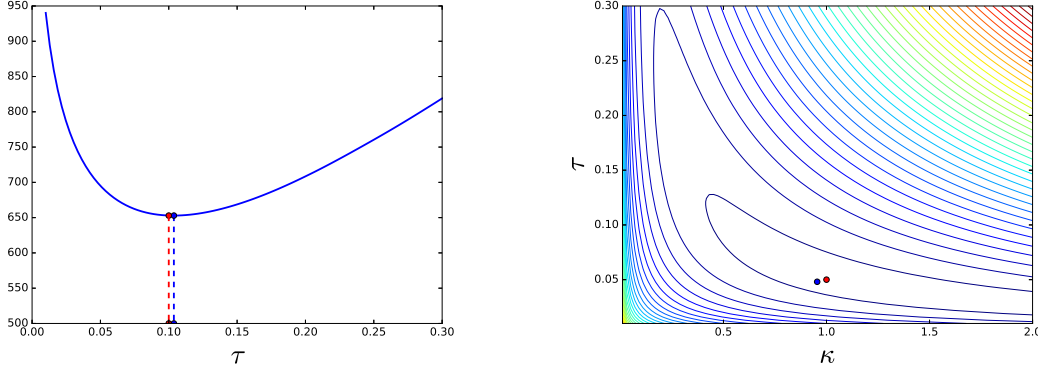
This is the *value function* of the shape parameters, after  $x$  has been minimized. For simple examples,  $\theta$  may have dimension 1 or 2, we can plot either the graph or the level sets of this function. We generate the samples  $\epsilon_i$  from distribution defined by quantile Huber function with  $\kappa = 1$  and  $\tau = 0.05$ , and plot  $\varrho(\theta)$  in Figure 3.

From Figure 3 (a), we can see that for the quantile penalty, the value function  $\varrho$  appears to be quasi-convex for this example; and we can expect to find the unique global minimum in  $x$  and  $\tau$ , since computing the projection require solving a convex problem. When  $\theta$  comprises both  $\tau$  and  $\kappa$  in (b), the joint objective is clearly nonconvex and may be more challenging for a local search (the level sets are stretched and bent). Nonetheless, there is a unique global minimum that is close to the true parameters; and this minimum was found by a local search.

### 3. First- and Second-Order Algorithms.

In this section, we consider first- and second-order methods for problems of type (4).

When  $\rho$  is smooth in  $x$  and  $\theta$ , we show how to apply the Proximal Alternating Linearized Minimization (PALM) algorithm (Bolte et al., 2014). The development is straightforward,



(a) Graph of quantile value function  $\varrho(\tau)$  (b) level sets of the QH value function  $\varrho(\tau, \kappa)$ .

Figure 3: Left panel: graph of value function  $\varrho(\tau)$ . Right panel: level sets of quantile huber (QH) value function  $\varrho(\tau, \kappa)$ . Blue dots show optimal parameter estimates, while red dots show true parameters.

but the log normalization constant  $\log[n_c(\theta)]$  must be treated carefully, as its gradient does not have a global Lipschitz constant.

Requiring smoothness in  $\rho$  is restrictive; and in particular eliminates the quantile example (5). The quantile penalty is not smooth, but it is piecewise linear. Interior point methods have been shown to be effective for convex problems of moderate scale (thousands of variables and data points) where  $\rho$  and  $g$  are nonsmooth piecewise linear-quadratic penalties (Aravkin et al., 2013). Examples include symmetric penalties (1-norm, quadratic) as well as asymmetric penalties, such as quantile and quantile Huber (Aravkin et al., 2014). All of these penalties are shown in detail in the supplementary materials. Our main algorithmic contribution is to extend this approach to the joint nonconvex inference problem (4).

### 3.1 PALM for inference and shape estimation

The PALM algorithm (Bolte et al., 2014) can be used to minimize any problem of form

$$\min_{x, \theta} H(x, \theta) + r_1(x) + r_2(\theta),$$

where  $H$  is  $C^1$ , with globally Lipschitz partial gradients, while the functions  $r_1$  and  $r_2$  are required to be only proper lower semicontinuous (in particular not necessarily convex, finite valued, or smooth). Even though  $\log[n_c(\theta)]$  is smooth (see Theorem 1), it must be relegated to  $r_2(\theta)$ , since otherwise it can easily violate the Lipschitz assumptions on  $H$ . Therefore, to apply PALM to (4), we take

$$H(x, \theta) = \sum_{i=1}^m \rho(y_i - \langle a_i, x \rangle; \theta), \quad r_1(x) = g(x), \quad r_2(\theta) = \delta_{\mathcal{D}}(\theta) + m \log[n_c(\theta)]. \quad (7)$$

Here  $\delta_{\mathcal{D}}$  is the indicator function for the set  $\mathcal{D}$ , ensuring  $\theta \in \mathcal{D}$ , and  $g$  is any ‘prox-friendly’ regularizer for  $x$ . The PALM algorithm is detailed in Algorithm 1. The steps  $c_k$  and  $d_k$  are obtained from Lipschitz constants of the (partial) gradients of  $H$ .

**Algorithm 1** PALM for (7)**Input:**  $A, y$ 

- 1: **Initialize:**  $x^0, \theta^0$
- 2: **while** not converge **do**
- 3:    $x^{k+1} \leftarrow \text{prox}_{\frac{1}{c_k} r_1} \left( x^k - \frac{1}{c_k} \nabla_x H(x^k, \theta^k) \right)$
- 4:    $\theta^{k+1} \leftarrow \text{prox}_{\frac{1}{d_k} r_2} \left( \theta^k - \frac{1}{d_k} \nabla_\theta H(x^{k+1}, \theta^k) \right)$

**Output:**  $x^k$  and  $\theta^k$ 

**Detail:** The prox operator of  $\log[n_c(\theta)]$  is not available in closed form for any examples of interest. However, the prox operator can be efficiently computed using the results of Theorem 1:

$$\text{prox}_{\frac{1}{d_k} r_2}(\phi) = \arg \min_{\theta \in \mathcal{D}} \frac{1}{2d_k} \|\theta - \phi\|^2 + \log[n_c(\theta)]. \quad (8)$$

In all examples of interest,  $\theta$  is low dimensional; so we compute (8) using Newton's method or an interior point method (when  $\mathcal{D}$  must be accounted for). This requires  $\nabla \log[n_c(\theta)]$  and  $\nabla^2 \log[n_c(\theta)]$ , which are calculated numerically using formulas (6).

The PALM algorithm is well suited to large-scale shape inference problems with smooth coupling of  $x$  and  $\theta$  in  $\rho$ . We use it for the self-tuning RPCA experiments in Section 5.

### 3.2 Interior point method for self-tuning piecewise linear-quadratic penalties

The restriction that  $\rho$  must be smooth in  $(x, \theta)$  is unsatisfying, given that one of the simplest examples of self-tuning penalties comes from the nonsmooth quantile loss. Here, we develop an interior point method for the quantile problem (5), as well as any other analogous problems for shape parameter estimation with PLQ penalties. The class includes many familiar losses (Huber, quantile, quantile Huber,  $\ell_2$  and  $\ell_1$ ). While many of these are nonsmooth, they all have smooth conjugate representations. Aravkin et al. (2013) used these representations to solve convex PLQ problems, including Lasso, support vector machine, and Huber regression. We extend the approach to solve nonconvex extended problems of form  $\min_{x, \theta \in \mathcal{D}} \rho(x; \theta) + \log[n_c(\theta)]$ .

The approach is limited to moderate problem dimensions<sup>1</sup>, but converges at a superlinear rate, and solves problems with nonsmooth coupling in  $(x, \theta)$ . We first review conjugate representations of PLQ penalties. The quantile Huber penalty (Figure 4) is the convex conjugate of the function  $\frac{1}{2}\|u\|^2 + \delta_{[-\kappa\tau, \kappa(1-\tau)]}(u)$ , For more examples, see the Appendix.

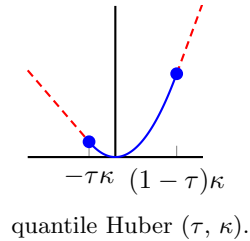


Figure 4: Quantile Huber  $(\tau, \kappa)$  penalty has conjugate representation

$$\sup_{u \in [-\kappa\tau, \kappa(1-\tau)]} ux - \frac{1}{2}u^2.$$

1. If  $A$  has dimensions  $m$  and  $n$ , interior point methods require  $O(n(m^2 + n^2))$  arithmetic operations, where  $n$  is the smaller dimension. This limits practical applications for large-scale problems; to go beyond  $2000 \times 2000$  with modest compute, some sort of special structure or technique (sparsity, preconditioning) is typically needed.

PLQ functions are closed under sums and affine compositions, and the generic PLQ object has can be expressed as the conjugate of  $\frac{1}{2}u^\top Mu + \delta_U(u)$ , evaluated at some input  $Br - \bar{b}$  Aravkin et al. (2013):

$$\rho(r, \theta; B, \bar{b}, C, \bar{c}, M) = \sup_u \left\{ u^\top (Br - \bar{b}) - \frac{1}{2} u^\top Mu \mid C^\top u \leq \bar{c} \right\} \quad (9)$$

where  $M \succeq 0$ , and  $U := \{u \mid C^\top u \leq \bar{c}\}$  is a polyhedral set with  $0 \in U$ . To incorporate shape penalty estimation, we allow  $\bar{b}$  and  $\bar{c}$  to be affine functions of  $\theta$ , and assume  $\mathcal{D}$  is also polyhedral:

$$\bar{b} = G^\top \theta + b, \quad \bar{c} = H^\top \theta + c, \quad \mathcal{D} = \{\theta \mid S^\top \theta \leq s\}.$$

Our goal now is to now solve a *saddle point* system that includes primal variables  $x$ , conjugate variables  $u$ , and shape parameters  $\theta$ :

$$\min_{x, S^\top \theta \leq s} \sup_{C^\top u \leq H^\top \theta + c} \left\{ u^\top [B(Ax - y) - G^\top \theta - b] - \frac{1}{2} u^\top Mu \right\} + m \log[n_c(\theta)] \quad (10)$$

For example, the self-tuning quantile penalty (5) (with  $\theta = \tau$ ) gives

$$\min_{x, \begin{bmatrix} 1 \\ 1 \\ -1 \end{bmatrix} \tau \leq \begin{bmatrix} 1 \\ 1 \\ 0 \end{bmatrix}} \sup_{\begin{bmatrix} 1 \\ -1 \end{bmatrix} u \leq -\begin{bmatrix} 1 \\ 1 \end{bmatrix} \tau + \begin{bmatrix} 1 \\ 0 \end{bmatrix}} u^\top (Ax - b) + m \log \left( \frac{1}{\tau} + \frac{1}{1 - \tau} \right).$$

Interior point (IP) methods apply damped Newton to a relaxation of the optimality conditions (10), see (Kojima et al., 1991; Nemirovskii and Nesterov, 1994; Wright, 1997). The relaxation can be derived by approximating indicator functions of the constraints using a log-barrier function with parameter  $\mu$ :

$$\delta_{\{(u, \theta) \mid C^\top u \leq H^\top \theta + c\}}(u, \theta) \approx -\mu \mathbf{1}^\top \log(c + H^\top \theta - C^\top u).$$

Note that as  $\mu \downarrow 0$ , the barriers approach true indicator functions for  $U$ . The barrier parameter  $\mu$  is aggressively decreased to a specified optimality criterion as the optimization proceeds. For fixed  $\mu$ , there is an associated approximate objective for (10), given by

$$\min_{x, S^\top \theta \leq s} \sup_u \left\{ u^\top [B(Ax - y) - G^\top \theta - b] - \frac{1}{2} u^\top Mu + \mu \mathbf{1}^\top \log(c + H^\top \theta - C^\top u) \right\} + m \log[n_c(\theta)] - \mu \mathbf{1}^\top \log(s - S^\top \theta) \quad (11)$$

And we apply the Lagrangian dual formulation for this objective,

$$\mathcal{L}_\mu(d_1, q_1, x, u, \theta) = u^\top [B(Ax - y) - G^\top \theta - b] - \frac{1}{2} u^\top Mu + \mu \mathbf{1}^\top \log(c + H^\top \theta - C^\top u) + m \log[n_c(\theta)] - \mu \mathbf{1}^\top \log(s - S^\top \theta) + q_1^\top (d_1 + S^\top \theta - s) \quad (12)$$

where  $q_1$  is the dual variable and  $d_1$  is the slack variable. By introducing another pair of dual-slack variable  $q_2$  and  $d_2$  for log-barrier function,

$$d_2 = c - C^\top u + H^\top \theta, \quad q_2 = \mu D_2^{-1} \mathbf{1}$$



where all the capital letters represent diagonal matrices with corresponding little letters vector as the diagonal. We could form the KKT system of (11),

$$F_\mu(z) = \begin{bmatrix} D_1 q_1 - \mu \mathbf{1} \\ d_1 + S^\top \theta - s \\ D_2 q_2 - \mu \mathbf{1} \\ B(Ax - y) - G^\top \theta - b - Mu - Cq_2 \\ A^\top B^\top u \\ -Gu + m \nabla \log[n_c(\theta)] + Sq_1 + Hq_2. \end{bmatrix} \quad (13)$$

The Jacobian matrix  $\nabla F_\mu$  of the system is given by

$$\nabla F_\mu(z) = \begin{bmatrix} Q_1 & D_1 & & & & \\ I & & & & & S^\top \\ & & D_2 & -Q_2 C^\top & & Q_2 H^\top \\ & & -C & -M & BA & -G^\top \\ & & & A^\top B^\top & & \\ & S & H & -G & & \nabla^2 \log[n_c(\theta)] \end{bmatrix} \quad (14)$$

Where  $z = [d_1, q_1, q_2, u, x, \theta]^\top$ . Notice that when  $\mu \downarrow 0$ , (13) will approach to the optimality condition of (10), Algorithm 2 shows the IP method.

---

**Algorithm 2** Interior point method for PLQ with  $\theta$  estimation

---

**Input:**  $A, y, B, b, C, c, G, H, S, s$

- 1: **Initialize:**  $z^0, \mu = 1$
- 2: **while** not converged **do**
- 3:    $p \leftarrow \nabla F_\mu(z^k)^{-1} F_\mu(z^k)$
- 4:    $\alpha \leftarrow \text{LineSearch}(z^k, p)$ , using merit function  $\|F_\mu(\cdot)\|$
- 5:    $z^{k+1} \leftarrow z^k - \alpha p$
- 6:    $\mu \leftarrow 0.1 \cdot$  (Average complementarity conditions)

**Output:**  $z^{k+1}$

---

Implementability of Algorithm 2 is analyzed in Theorem 3.

**Theorem 3 (Implementability)** *Let  $T_2 = Q_2^{-1} D_2$ . Suppose the following conditions are satisfied:*

- $\text{null}(M) \cap \text{null}(C^\top) = \{0\}$
- $\text{null}(BA) = \{0\}$
- $\text{null}(\nabla^2 \log[n_c(\theta)]) \cap \text{null}(S^\top) \cap \text{null}(H^\top) \cap \text{null}(-G^\top + CT_2^{-1}H^\top) = \{0\}$

*for every  $\theta \in \mathcal{D}$ . Then Algorithm 2 is implementable; in particular  $p$  in step 3 can always be found. Moreover, we could replace the third condition by a stronger assumption that is if  $\log[n_c(\theta)]$  is strongly concave.*

The proof appears in the appendix.

#### 4. Synthetic Data Experiments

We illustrate the proposed approach using a linear regression example. We consider a data set contaminated by asymmetric errors and outliers, two features captured by the quantile Huber penalty (Figure 4). The slope  $\tau$  controls for the asymmetry, while the threshold  $\kappa$  detects the point beyond which a residual might be classified as an ‘outlier’. The goal of the experiment is to simultaneously learn the regression model parameters  $x$  as well as obtain the correct  $\tau$  and  $\kappa$ . Simple residual analysis is not possible *a priori*, since the model parameters  $x$  are also unknown.

When  $\kappa > 0$  in quantile Huber,  $\rho(x; \theta)$  is smooth, and we can use the PALM algorithm from Section 3.1. The quantile penalty is also PLQ, so we can also apply the proposed IP method from Section 3.2. We use both and compare their performance.

The primal form for the quantile Huber penalty is

$$\rho(r; \theta) = \begin{cases} -\tau\kappa r - \frac{(\tau\kappa)^2}{2}, & r < -\tau\kappa \\ \frac{1}{2}r^2, & r \in [-\tau\kappa, (1-\tau)\kappa] \\ (1-\tau)\kappa r - \frac{((1-\tau)\kappa)^2}{2}, & r > (1-\tau)\kappa. \end{cases} \quad (15)$$

We must choose a parametrization in terms of  $\theta$ . One option would be to take  $\theta = [\tau, \kappa]^T$ . But this parametrization would violate assumptions of both the first- and second-order approaches in Section 3. Indeed,  $\nabla_{\theta}\rho(r; \theta)$  would not have a global Lipschitz constant, so we could not use PALM. Similarly, we could not write the conjugate representation (10) using affine functions of  $\theta$ . Looking carefully at either (15) or (10), we instead choose  $\theta_1 = \tau\kappa, \theta_2 = \tau(1-\kappa)$ . The only requirement on these parameters is that they are each non-negative.

The primal objective can be written as

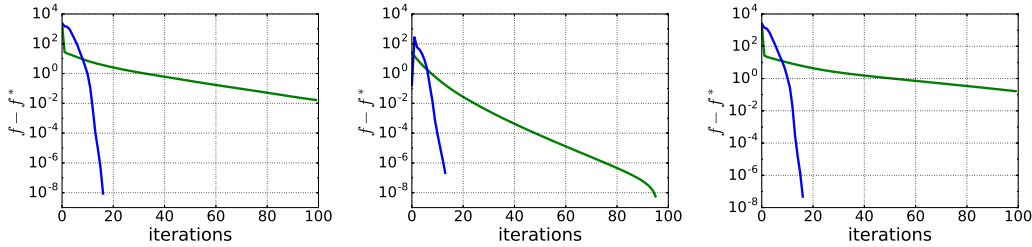
$$\min_{x, \theta \geq 0} \rho(Ax - y; \theta) + m \log[n_c(\theta)].$$

where  $A \in \mathbb{R}^{m \times n}$  is the design matrix,  $x \in \mathbb{R}^n$  is the model parameter vector, and  $y \in \mathbb{R}^m$  is the observed data vector contaminated by outliers. From Theorem 1,  $n_c(\theta)$  is  $\mathcal{C}^2$  smooth. From Theorem 2, the objective in  $\theta$  is the sum of a concave term  $\rho(Ax - y; \theta)$  and a convex term  $m \log(n_c(x))$ . The joint problem in  $(x, \theta)$  is nonconvex. Nonetheless, both first- and second-order methods from Section 3 can be applied to solve the problem.

We generate synthetic data with  $m = 1000$ ,  $n = 50$ , and generate the elements of  $A \in \mathbb{R}^{m \times n}$  from a standard Gaussian random distribution. The measurement errors are sampled from quantile Huber distributions, to verify that the approach is able to recover ‘ground truth’ values for  $(\tau, \kappa)$  parameters. We denote ground truth parameters as  $x_t, \tau_t, \kappa_t$ , while  $x^*, \tau^*, \kappa^*$  are the solutions obtained by solving (4). We provide two reference solutions:  $x_{LS}$  is the least square solution, and  $x_M$  is the solution obtained by solving  $\|Ax - b\|_1$ . For each  $\kappa$  and  $\tau$  setting, we run the simulation 10 times, and show the average of the results in Table 1. Results shown are obtained by the IP method.

$[\tau_t, \kappa_t]$	$[\tau^*, \kappa^*]$	$\ x^* - x_t\ /\ x_t\ $	$\ x_{LS} - x_t\ /\ x_t\ $	$\ x_M - x_t\ /\ x_t\ $
[0.1,1.0]	[0.090,1.165]	0.142	0.412	0.255
[0.2,1.0]	[0.196,1.067]	0.101	0.155	0.125
[0.5,1.0]	[0.501,0.948]	0.077	0.122	0.085
[0.8,1.0]	[0.807,1.041]	0.092	0.189	0.113
[0.9,1.0]	[0.912,1.173]	0.119	0.379	0.359

Table 1: Joint inference of the shape and model parameters for the quantile Huber loss.

Figure 5: Convergence history (iterations) for PALM (green) and interior point method (blue). Three experiments are shown, for  $\tau = 0.1, 0.5$ , and  $0.9$ . The proposed IP method converges in fewer than 20 iterations in all cases.

The maximum likelihood formulation correctly recovers the shape parameters  $(\theta, \tau)$  in the context of solving a regression problem. Moreover, the solution  $x^*$  obtained from the self-tuned regression is always better compared to reference solutions; and the improvement increases as measurement errors become more biased ( $\tau$  close to 0 or to 1).

We also compared the performance of PALM and IP, in terms of iterations. The result (for three selections of  $\tau$  and  $\kappa$  values) is shown in Figure 5. The IP method takes very few iterations to converge. However, the cost of each IP iteration grows cubically in the minimum of  $(n, m)$ , and only quadratically for each PALM iteration. In case of nonsmooth  $\rho$ , PALM cannot be applied.

Here, we replicate the experiment for the quantile penalty alone, to show that the IP approach indeed handles fully nonsmooth problems. We choose  $m = 500$ ,  $n = 50$ , same way generate  $A \in \mathbb{R}^{m \times n}$  and  $x_t \in \mathbb{R}^n$  with Section 4. And then we generate independent samples from distribution defined by quantile function. The result is shown in the Table 2.

Conclusions similar to self-tuning quantile Huber can be drawn here. We recover  $\tau$  accurately and when  $\tau$  is close to 0 and 1, our solution is much better than least squares and  $\ell_1$  norm solutions.

## 5. Self-Tuning RPCA

Robust principal component analysis (RPCA) has applications to alignment of occluded images (Peng et al., 2012), scene triangulation (Zhang et al., 2012), model selection (Chan-

$\tau_t$	$\tau^*$	$\ x^* - x_t\ /\ x_t\ $	$\ x_{LS} - x_t\ /\ x_t\ $	$\ x_{l_1} - x_t\ /\ x_t\ $
0.1	0.096	0.253	0.749	0.439
0.2	0.216	0.139	0.191	0.160
0.5	0.491	0.134	0.134	0.134
0.8	0.794	0.136	0.341	0.208
0.9	0.903	0.242	0.542	0.475

Table 2: Joint inference of the shape and model parameters for the quantile penalty.

drasekaran et al., 2009), face recognition (Turk and Pentland, 1991) and document indexing (Candès et al., 2011).

We develop a self-tuning background separation approach. Given a sequence of images<sup>2</sup>, our goal is to separate the moving objects from the background. We pick 202 images from the data set, convert them to grey scale and reshape them as column vectors of matrix  $Y \in \mathbb{R}^{20480 \times 202}$ . We model the data  $Y$  as the sum of low rank component  $L$  of  $Y$  and sparse noise  $S$ ; we expect moving objects to be captured by  $S$ .

The stable version of RPCA is equivalent to regularized Huber regression:

$$\min_{L, S} \frac{1}{2} \|L + S - Y\|_F^2 + \kappa \|S\|_1 + \lambda \|L\|_* = \min_L \rho_\kappa(Y - L) + \lambda \|L\|_*. \quad (16)$$

The equality is obtained by partially minimizing in  $S$ . We can simplify (2) further by modeling  $L = U^T V$ , where  $U$  and  $V$  are matrices with  $k \ll \min(m, n)$  columns. The resulting objective is given by

$$\min_{U, V} \sum_{i, j} \rho(\langle U_i, V_j \rangle - Y_{i, j}; \kappa)$$

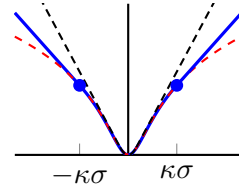
where  $U \in \mathbb{R}^{k \times m}$  and  $V \in \mathbb{R}^{k \times n}$  and  $U_i, V_j$  are the column vectors. In this experiment we choose  $k = 2$ . Shape parameter  $\kappa$  play a key role for the performance of the formulation: a bad choice of  $\kappa$  translates into poor separation, see Figure 7 (a). Cross-validation is computationally expensive for RPCA, so we can instead automatically tune  $\kappa$  as we fit  $U$  and  $V$ .

In order to get the result in Figure 7 (b), we introduce a variance parameter  $\sigma$  for the Huber penalty to automatically estimate the right scale of the residual. The joint  $(\kappa, \sigma)$  parametrization is given by

$$\rho(r; [\kappa, \sigma]) = \begin{cases} \kappa|r|/\sigma - \kappa^2/2, & |r| > \kappa\sigma \\ r^2/(2\sigma^2), & |r| \leq \kappa\sigma, \end{cases}$$

with the resulting self-tuning RPCA formulation (solved by Algorithm 1):

$$\min_{U, V, \kappa > 0, \sigma > 0} \sum_{i, j} \rho(\langle U_i, V_j \rangle - Y_{i, j}; [\kappa, \sigma]) + mn \log[n_c([\kappa, \sigma])].$$


 Figure 6: Huberized Student's  $t$  (thick blue) interpolates between Student's  $t$  (red dash) and Huber (black dash).

2. Publicly available at <http://vis-www.cs.umass.edu/~narayana/castanza/I2Rdataset/>

The result is shown in Figure 7(b). As the optimization proceeds,  $\kappa, \sigma \rightarrow 0^+$  with a fixed ratio  $\alpha = \kappa/\sigma$ . The self-tuning Huber becomes the scaled 1-norm, recovering the original RPCA formulation (Candès et al., 2011). The result in Figure 7(b) is an improvement over the result with  $(\kappa, \sigma)$  fixed at the initial values in Figure 7(a).

The weakness of the Huber is that the  $\kappa$  has to work well for residuals near the origin as well as in the tail. The self-tuning approach makes it easy to create and adapt new penalties. To get additional flexibility, we introduce an inflection point; letting the ‘slope’ near the origin be different from slopes in the tails. The Huberized Student’s  $t$  penalty is shown in Figure 6, and detailed below:

$$\rho(r; [\kappa, \sigma]) = \begin{cases} \frac{2\kappa}{\sigma(\kappa^2+1)}(|r| - \kappa\sigma) + \log(1 + \kappa^2), & |r| > \kappa\sigma \\ \log(1 + r^2/\sigma^2), & |r| \leq \kappa\sigma \end{cases} \quad (17)$$

Penalty (17) is flexible, in the sense that behavior for large residuals and small ones is decoupled. When we self-tune this new penalty, the additional flexibility indeed improves on the self-tuned Huber, recovering the results shown in Figure 7(d). It is clear the self-tuning approach succeeds, as the Huberized Student’s  $t$  result at the initial  $\kappa, \sigma$  values is useless (Figure 7(c)).

In this data set, the advantage of self-tuned Huberized Student’s  $t$  over self-tuned Huber may not be that obvious. We also apply our approach to Escalator data set<sup>3</sup>. This data set is less noisy than the first, but contains multiple moving objects. We select a time window with 200 pictures, and  $Y \in \mathbb{R}^{20800 \times 200}$ , and apply the huber and Huberized Student’s  $t$  to this data set, with results shown in Figure 8.

We can see that there are a lot of artifacts in the self-tuned Huber penalty result, e.g., the escalator stairs and shadow of people. Instead the result for self-tuned Huberized Student’s  $t$  is much cleaner and we isolate the moving people successfully. All of these results are achieved with fully automatic parameter tuning.

Here, we use self-tuning Huber and self-tuning Huberized Student’s  $t$  penalties. Looking at Figure 8, the self-tuned Huber has stronger signal but includes more background; the picture looks better to the eye but a closer examination reveals parts of the escalator are present. The self-tuned Huberized Student’s  $t$  has weaker  $S$  which is harder to see; but actually gives a much better result.

To get more insights into the problem, we also look at the empirical distribution of the residual. In Figure 9, the light blue line denote the empirical CDF for the residual ( $R = Y - U^T V$ ), red dashed line is the the best Huberized Student’s  $t$  fit, blue dashed line is the best  $\ell_2$  fit and green dashed line is the best  $\ell_1$  fit. We can see that Huberized Student’s  $t$  has a perfect fit, and in particular is much better than  $\ell_1$  and  $\ell_2$ .

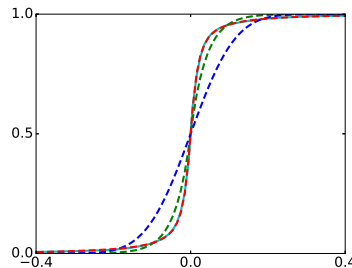


Figure 9: Best fit for residual empirical CDF

3. Publicly available at <http://vis-www.cs.umass.edu/~narayana/castanza/I2Rdataset/>

## 6. Conclusions

We introduced a method for self-tuning error penalties, incorporates the log of the normalization constant (a function of the shape parameters) into an extended joint inference problem. Results with synthetic data as well as real data show promise. Future research includes designing innovative ‘flexible’ penalties and automatically adapting them to different applications.

## Appendix A. Proof of Theorem 1

**Proof** From Assumption 1, we know that for any  $\theta_0 \in \mathcal{D}$ ,  $\nabla_\theta \exp[\rho(r; \theta_0)]$  and  $\nabla_\theta^2 \exp[\rho(r; \theta_0)]$  exist for almost every  $r \in \mathbb{R}$ . For any  $h$  such that  $\|h\|$  is small enough to make  $\theta_0 + h$  stay in the neighborhood of  $\theta_0$ . By applying mean value theorem, we have,

$$\begin{aligned} n_c(\theta_0 + h) - n_c(\theta_0) &= \int_{\mathbb{R}} \exp[-\rho(r; \theta_0 + h)] - \exp[-\rho(r; \theta_0)] dr \\ &= \int_{\mathbb{R}} \langle \nabla_\theta \exp[-\rho(r; \bar{\theta})], h \rangle dr \\ \Rightarrow \frac{n_c(\theta_0 + h) - n_c(\theta_0)}{\|h\|} &= \int_{\mathbb{R}} \left\langle \nabla_\theta \exp[-\rho(r; \bar{\theta})], \frac{h}{\|h\|} \right\rangle dr \end{aligned}$$

where  $\bar{\theta}$  lie in segment with the end points  $\theta_0$  and  $\theta_0 + h$ . For the first and third assumptions in the theorem, we could apply the dominant convergence theorem and get,

$$\begin{aligned} \lim_{h \rightarrow 0} \frac{n_c(\theta_0 + h) - n_c(\theta_0)}{\|h\|} &= \lim_{h \rightarrow 0} \int_{\mathbb{R}} \left\langle \nabla_\theta \exp[-\rho(r; \bar{\theta})], \frac{h}{\|h\|} \right\rangle dr \\ &= \int_{\mathbb{R}} \lim_{h \rightarrow 0} \left\langle \nabla_\theta \exp[-\rho(r; \bar{\theta})], \frac{h}{\|h\|} \right\rangle dr \\ &= \int_{\mathbb{R}} \langle \nabla_\theta \exp[-\rho(r; \theta_0)], v \rangle dr \\ &= \left\langle \int_{\mathbb{R}} \nabla_\theta \exp[-\rho(r; \theta_0)] dr, v \right\rangle \end{aligned}$$

where we set  $h = \alpha v$  and let  $\alpha \rightarrow 0^+$  and keep  $v$  fix as an unit vector. From the definition of the gradient we know that,

$$\nabla n_c(\theta_0) = \int_{\mathbb{R}} \nabla_\theta \exp[-\rho(r; \theta_0)] dr.$$

Follow the same steps we could also show  $\nabla^2 n_c(\theta_0)$  exists and satisfies,

$$\nabla^2 n_c(\theta_0) = \int_{\mathbb{R}} \nabla_\theta^2 \exp[-\rho(r; \theta_0)] dr.$$

■

## Appendix B. Proof of Theorem 3

**Proof** By applying row operations to (14) we obtain a block upper triangular system,

$$\nabla F_\mu(z) \rightarrow \left[ \begin{array}{c|c|c|c|c|c} Q_1 & D_1 & & & & \\ \hline & T_1 & & & & S^\top \\ \hline & & T_2 & -C^\top & & H^\top \\ \hline & & & T_3 & BA & -G^\top + CT_2^{-1}H^\top \\ \hline & & & & T_4 & -A^\top B^\top T_3^{-1}(-G^\top + CT_2^{-1}H^\top) \\ \hline & & & & & T_5 \end{array} \right]$$

where,

$$\begin{aligned} T_1 &= Q_1^{-1} D_1 \\ T_2 &= Q_2^{-1} D_2 \\ T_3 &= -M - CT_2^{-1}C^\top \\ T_4 &= -A^\top B^\top T_3^{-1}BA \\ T_5 &= \nabla^2 \log[n_c(\theta)] - ST_1^{-1}S^\top - HT_2^{-1}H^\top \\ &\quad - (-G + HT_2C^\top)(T_3^{-1} + T_3^{-1}BAT_4^{-1}A^\top B^\top T_3^{-1})(-G^\top + CT_2^{-1}H^\top) \end{aligned}$$

$\nabla F_\mu$  is invertible if and only if  $Q_1, T_i, i = 1, 2, 3, 4, 5$  are invertible. Since we guarantee  $q_1, q_2, d_2 > 0$  through line search,  $Q_1, T_1$  and  $T_2$  are invertible. It's easy to see that

- if  $\text{null}(M) \cap \text{null}(C^\top) = \{0\}$ ,  $T_3$  is invertible.
- if  $\text{null}(BA) = \{0\}$ ,  $T_4$  is invertible.
- if  $\text{null}(\nabla^2 \log[n_c(\theta)]) \cap \text{null}(S^\top) \cap \text{null}(H^\top) \cap \text{null}(-G^\top + CT_2^{-1}H^\top) = \{0\}$  and above two points hold,  $T_5$  is invertible.

Moreover, if  $\log[n_c(\theta)]$  is strongly concave,  $T_5 \prec 0$  which is invertible. Then we proof the invertibility of  $\nabla F_\mu$  which guarantee the implementability of Algorithm 2.  $\blacksquare$

## Appendix C. Conjugate Representations of Various Penalties

We provide examples of common penalties used in statistical modeling, machine learning, and inverse problems with their conjugate representations:

1. The least squares penalty (Fig. 10(a))  $\frac{1}{2}x^2 = \sup_u \{ux - \frac{1}{2}u^2\}$ .
2. The quantile penalty (Fig. 2(b))  $q_\tau(x) = \sup_{u \in [-\tau, (1-\tau)]} \{ux\}$ .
3. The hinge loss (Fig. 10(d))  $h_\epsilon(x) = \sup_{u \in [-\tau, (1-\tau)]} \{u(x - \epsilon)\}$ .

4. The Huber function (Fig. 2(a))  $h_\kappa(x) = \sup_{u \in [-\kappa, \kappa]} \{ux - \frac{1}{2}u^2\}$ .
5. The quantile Huber (Fig. 10(e))  $h_{\tau, \kappa}(x) = \sup_{u \in [-\kappa\tau, \kappa(1-\tau)]} \{ux - \frac{1}{2}u^2\}$ .
6. The Vapnik penalty (Fig. 10(f))  $\rho_\epsilon(x) = \sup_{u \in [0, 1]^2} \left\{ \left\langle \begin{bmatrix} 1 \\ -1 \end{bmatrix} x - \begin{bmatrix} \epsilon \\ \epsilon \end{bmatrix}, u \right\rangle \right\}$ .
7. Smooth insensitive loss (Fig. 10(g))  $\rho_\epsilon^h(x) = \sup_{u \in [0, 1]^2} \left\{ \left\langle \begin{bmatrix} 1 \\ -1 \end{bmatrix} x - \begin{bmatrix} \epsilon \\ \epsilon \end{bmatrix}, u \right\rangle - \frac{1}{2}u^T u \right\}$ .
8. The elastic net penalty (Fig. 10(h))  $\rho(x) = \sup_{u \in [0, 1] \times \mathbb{R}} \left\{ \left\langle \begin{bmatrix} 1 \\ 1 \end{bmatrix} x, u \right\rangle - \frac{1}{2}u^T \begin{bmatrix} 0 & 0 \\ 0 & 1 \end{bmatrix} u \right\}$ .
9. Hybrid loss (Fig. 10(b))  $h_\epsilon(x) = \sup_{u \in [-\epsilon^{-1}, \epsilon^{-1}]} \left\{ xu - \left( 1 - \sqrt{1 - (u\epsilon)^2} \right) \right\}$ .
10. Logistic loss (Fig. 10(c))  $h_a(x) = \sup_{u \in [0, a]} \left\{ xu - \frac{u}{a} \log \left( \frac{u}{a} \right) - \left( 1 - \frac{u}{a} \right) \log \left( 1 - \frac{u}{a} \right) \right\}$ .



## References

- Aleksandr Aravkin, Aurelie Lozano, Ronny Luss, and Prabhajan Kambadur. Orthogonal matching pursuit for sparse quantile regression. In *Data Mining (ICDM), 2014 IEEE International Conference on*, pages 11–19. IEEE, 2014.
- Aleksandr Y. Aravkin, James V. Burke, and Gianluigi Pillonetto. Sparse/robust estimation and kalman smoothing with nonsmooth log-concave densities: Modeling, computation, and theory. *Journal of Machine Learning Research*, 14:2689–2728, 2013. URL <http://jmlr.org/papers/v14/aravkin13a.html>.
- Anil K Bera, Antonio F Galvao, Gabriel V Montes-Rojas, and Sung Y Park. Asymmetric laplace regression: Maximum likelihood, maximum entropy and quantile regression. *Journal of Econometric Methods*, 5(1):79–101, 2016.
- James Bergstra and Yoshua Bengio. Random search for hyper-parameter optimization. *Journal of Machine Learning Research*, 13(Feb):281–305, 2012.
- James S Bergstra, Rémi Bardenet, Yoshua Bengio, and Balázs Kégl. Algorithms for hyper-parameter optimization. In *Advances in Neural Information Processing Systems*, pages 2546–2554, 2011.
- Jérôme Bolte, Shoham Sabach, and Marc Teboulle. Proximal alternating linearized minimization for nonconvex and nonsmooth problems. *Mathematical Programming*, 146(1-2): 459–494, 2014.
- Stephen Boyd and Lieven Vandenberghe. *Convex optimization*. Cambridge university press, 2004.
- Emmanuel J Candès, Xiaodong Li, Yi Ma, and John Wright. Robust principal component analysis? *Journal of the ACM (JACM)*, 58(3):11, 2011.
- Venkat Chandrasekaran, Sujay Sanghavi, Pablo A Parrilo, and Alan S Willsky. Sparse and low-rank matrix decompositions. *IFAC Proceedings Volumes*, 42(10):1493–1498, 2009.
- Frank Hutter, Holger H Hoos, and Kevin Leyton-Brown. Sequential model-based optimization for general algorithm configuration. In *International Conference on Learning and Intelligent Optimization*, pages 507–523. Springer, 2011.
- Aaron Klein, Stefan Falkner, Simon Bartels, Philipp Hennig, and Frank Hutter. Fast bayesian optimization of machine learning hyperparameters on large datasets. *arXiv preprint arXiv:1605.07079*, 2016.
- M Kojima, N Megiddo, T Noma, and A Yoshise. *A Unified Approach to Interior Point Algorithms for Linear Complementarity Problems*, volume 538 of *Lecture Notes in Computer Science*. Springer Verlag, Berlin, Germany, 1991.
- Lisha Li, Kevin Jamieson, Giulia DeSalvo, Afshin Rostamizadeh, and Ameet Talwalkar. Hyperband: A novel bandit-based approach to hyperparameter optimization. *arXiv preprint arXiv:1603.06560*, 2016.

- A Nemirovskii and Y Nesterov. *Interior-Point Polynomial Algorithms in Convex Programming*, volume 13 of *Studies in Applied Mathematics*. SIAM, Philadelphia, PA, USA, 1994.
- Yigang Peng, Arvind Ganesh, John Wright, Wenli Xu, and Yi Ma. Rasl: Robust alignment by sparse and low-rank decomposition for linearly correlated images. *IEEE Transactions on Pattern Analysis and Machine Intelligence*, 34(11):2233–2246, 2012.
- Karthikeyan Natesan Ramamurthy, Aleksandr Y Aravkin, and Jayaraman J Thiagarajan. Automatic inference of the quantile parameter. *arXiv preprint arXiv:1511.03990*, 2015.
- Jasper Snoek, Hugo Larochelle, and Ryan P Adams. Practical bayesian optimization of machine learning algorithms. In *Advances in neural information processing systems*, pages 2951–2959, 2012.
- Shiyi Tu, Min Wang, and Xiaoqian Sun. Bayesian variable selection and estimation in maximum entropy quantile regression. *Journal of Applied Statistics*, 44(2):253–269, 2017. doi: 10.1080/02664763.2016.1168369. URL <http://dx.doi.org/10.1080/02664763.2016.1168369>.
- Matthew A Turk and Alex P Pentland. Face recognition using eigenfaces. In *Computer Vision and Pattern Recognition, 1991. Proceedings CVPR’91., IEEE Computer Society Conference on*, pages 586–591. IEEE, 1991.
- S J Wright. *Primal-Dual Interior-Point Methods*. Siam, Englewood Cliffs, N.J., USA, 1997.
- Keming Yu and Rana A Moyeed. Bayesian quantile regression. *Statistics & Probability Letters*, 54(4):437–447, 2001.
- Zhengdong Zhang, Arvind Ganesh, Xiao Liang, and Yi Ma. Tilt: Transform invariant low-rank textures. *International journal of computer vision*, 99(1):1–24, 2012.



(a) Huber with fixed  
 $\kappa = 2 \times 10^{-3}, \sigma = 1$ .



(b) Self-tuned Huber  
initial:  $\kappa = 2 \times 10^{-3}, \sigma = 1$   
final:  $\kappa = 1.94 \times 10^{-2}, \sigma = 8.28 \times 10^{-4}$

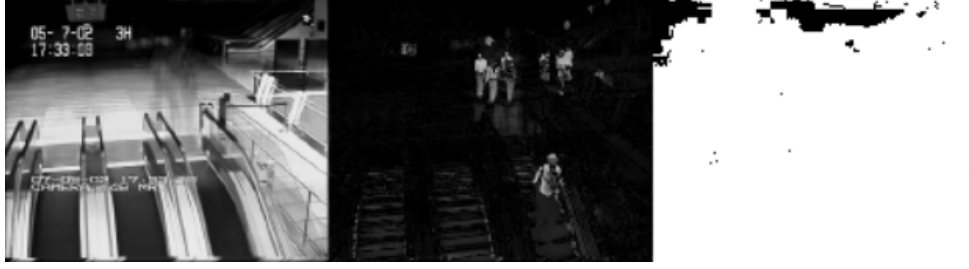


(c) Huberized Student's  $t$  with fixed  
 $\kappa = 8, \sigma = 0.1$



(d) Self-tuned Huberized Student's  $t$   
initial:  $\kappa = 8, \sigma = 0.1$   
final:  $\kappa = 7.64, \sigma = 2.24 \times 10^{-2}$

Figure 7: RPCA background separation: self-tuning automatically discovers shape parameters to produce desired result. Recovered backgrounds and foregrounds are in the top and bottom rows.



(a) self-tuned Huber  
 initial:  $\kappa = 0.02$ ,  $\sigma = 0.02$   
 final:  $\kappa = 7.48 \times 10^{-3}$ ,  $\sigma = 3.49 \times 10^{-4}$



(b) self-tuned Huberized Student's  $t$   
 initial:  $\kappa = 10$ ,  $\sigma = 2 \times 10^{-2}$   
 final:  $\kappa = 23.2$ ,  $\sigma = 1.66 \times 10^{-2}$

Figure 8: Background separation with the Escalator data. First column is the background, second column is the foreground, third column is the binary plot of the foreground.

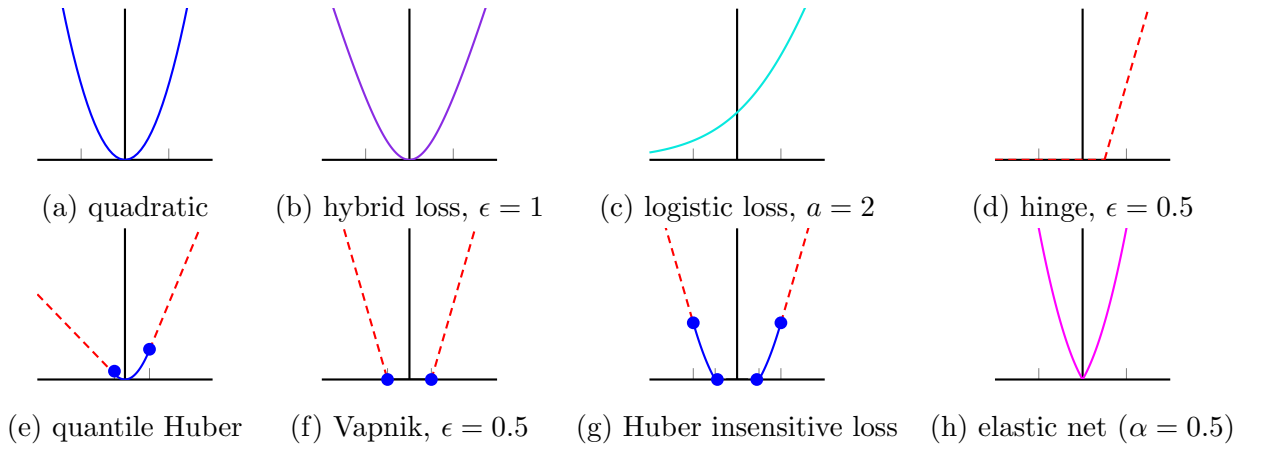


Figure 10: Eight common penalties frequently used in machine learning. Huber and quantile losses are shown in Fig. 2.